Role of contact-angle hysteresis for fluid transport in wet granular matter

Roman Mani,[1,*] Ciro Semprebon,[2] Dirk Kadau,[1] Hans J. Herrmann,[1,3] Martin Brinkmann,[2,4] and Stephan Herminghaus[2]

[1]*Computational Physics for Engineering Materials, ETH Zurich, 8093 Zurich, Switzerland*

[2]*Max Planck Institute for Dynamics and Self-Organisation, 37077 Göttingen, Germany*

[3]*Departamento de Física, Universidade Federal do Ceará, Fortaleza, Ceará 60451-970, Brazil*

[4]*Experimental Physics, Saarland University, 66123 Saarbrücken, Germany*

(Received 10 March 2014; revised manuscript received 9 October 2014; published 30 April 2015)

The stability of sand castles is determined by the structure of wet granulates. Experimental data on the size distribution of fluid pockets are ambiguous with regard to their origin. We discovered that contact-angle hysteresis plays a fundamental role in the equilibrium distribution of bridge volumes, and not geometrical disorder as commonly conjectured. This has substantial consequences on the mechanical properties of wet granular beds, including a history-dependent rheology and lowered strength. Our findings are obtained using a model in which the Laplace pressures, bridge volumes, and contact angles are dynamical variables associated with the contact points. While accounting for contact line pinning, we track the temporal evolution of each bridge. We observe a crossover to a power-law decay of the variance of capillary pressures at late times and a saturation of the variance of bridge volumes to a finite value connected to contact line pinning. Large-scale simulations of liquid transport in the bridge network reveal that the equilibration dynamics at early times is well described by a mean-field model. The spread of final bridge volumes can be directly related to the magnitude of contact-angle hysteresis.

DOI: 10.1103/PhysRevE.91.042204 PACS number(s): 45.70.−n, 47.55.nb, 47.55.nk, 47.55.np

I. INTRODUCTION

Our daily life is strongly affected by the mechanical properties of wet granulates, be it through the stability of the soil on which we construct our buildings or the consistency of the food we enjoy. The structure of the fluid interfaces in a wet granular bed essentially determines the strength of capillary cohesion and thus plays a key role in the prediction and mitigation of devastating events such as landslides or the clogging of industrial pipes [1,2]. For a thorough understanding, a realistic model of fluid movement is indispensable: The capillary pressure-driven fluid transport in wet granulates [3,4] changes the fluid distribution, which in turn suggests that the mechanical properties are affected by fluid displacement.

Indeed, shear thinning, for example, is observed for partially saturated beds of glass beads [1,5,6] due to a delayed reconfiguration of fluid interfaces. Knowledge about the evolution of the fluid distribution in the granular assembly is relevant to many industrial processes that involve coating of powders and grains [7], or mixing additives with particulate materials [8,9]. The precise microscopic features that determine the nature of the equilibration and fluid transport processes are yet largely unexplored.

In this article, we discover in simulations of the fluid equilibration process in a bed of spherical beads that contact line pinning can have a profound effect on the evolution of capillary bridge volumes. In agreement with the majority of experiments on fluid transport and pressure equilibration in wet granular beds [3,4,6,10], we consider the wetting fluid to be the minority phase forming capillary bridges at grain contacts or in narrow gaps between neighboring grains. Our simulations demonstrate that contact-angle hysteresis broadens the distribution of final bridge volumes while the polydispersity of bead radii and the distribution of gap separations in the granular bed appear to play only a minor role. The present approach accounts for the discreteness of the bridge network and incorporates the history dependence of the bridge shape caused by contact-angle hysteresis.

Combining the model for fluid transport with the contact dynamics (CD) algorithm [11–14] allows us to simulate the motion of beads due to an external driving and the redistribution of liquid after the external energy input has been stopped. In this way, a direct comparison of our numerical results to the evolution of bridge volumes using x-ray microtomography imaging of fluid distribution measured by Scheel *et al.* [4,10] is possible. In these experiments, vertical shaking of the granular bed was employed to distribute the wetting liquid on the surface of the beads. Shortly after the agitation of the wet granular bed (e.g., by stirring of shaking) has been stopped, the surfaces of the beads are covered with a "thick" macroscopic film of the wetting fluid [6]. Frequent closing and opening of contacts leads to a uniform distribution on the beads since the time scale of collisions is typically much smaller than time scales of viscous flows on the surface of the beads or of diffusion through the continuous fluid phase.

After the beads have settled into stable positions in the bead pack, the wetting fluid starts of flow to the points of closest proximity of opposing bead surfaces, forming macroscopic capillary bridges. At the end of this process, the liquid volume varies from bridge to bridge reflecting both the disorder in the bead pack and the distribution of fluid patches on the beads immediately after shaking.

The initial regime of bridge formation is followed by an equilibration of capillary pressure, which must involve an exchange of wetting fluid between neighboring bridges. In this "equilibration regime," the majority of the wetting fluid will be contained in macroscopic capillary bridges; cf. the sketch in Fig. 1. In the present work, we will focus on the

*manir@ethz.ch

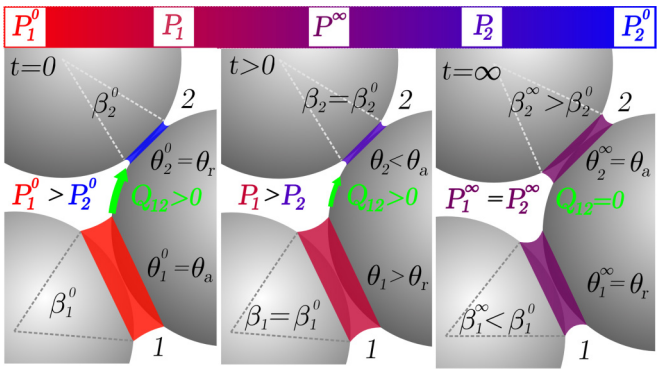

FIG. 1. (Color online) Effect of contact-angle hysteresis on the equilibration dynamics of two capillary bridges labeled $i = 1,2$ between beads with identical radii in mechanical contact.

collective evolution of bridge volumes in the equilibration regime where we assume that volume conservation holds for the wetting fluid. Our model for equilibration dynamics is based on the assumption that the fluid transport is entirely driven by differences in the local capillary pressure. For wetting liquids with a low vapor pressure, this transport proceeds mainly through thin wetting films in the roughness of the beads [3,6]. A diffusive transport through the vapor phase has to be considered for volatile liquids that exhibit a sufficiently high vapor pressure [15,16].

The central aim of the present work is to quantify the impact of contact-angle hysteresis and polydispersity of the particles in the granular bed onto the equilibration of bridge volumes. In particular, we address the question for typical time scales of the transport processes. These time scales of capillary pressure equilibration play an important role in the rheology of partially saturated wet granular beds.

II. PHYSICAL MODEL

For simplicity, we consider the wetting liquid that forms the capillary bridges (minority phase) to be surrounded by a continuous vapor phase (majority phase). Analogous statements can be obtained for binary mixtures of partially miscible liquids where the minority phase is a wetting liquid phase while the majority phase is a non-wetting liquid.

Throughout the following considerations, we will neglect contributions of the hydrostatic pressure to the pressure difference $P \equiv p_l - p_v$ between liquid (l) and vapor (v). Hence, the capillary pressure P is the same in every point of the liquid-vapor interface. Provided a uniform interfacial tension γ, the Young-Laplace equation

$$P = 2H\gamma \tag{1}$$

implies that the interface is a surface of constant mean curvature H. The mean curvature H is the sum of the two principal curvatures κ_1 and κ_2 in a respective point of the interface.

The influence of gravity or buoyancy on the capillary pressure P will become apparent whenever the maximal difference in hydrostatic pressure is of the order or exceeds γ/R_0, where R_0 is the average bead radius. This is the case if the vertical extension of the system becomes comparable, or exceeds the length

$$L_\perp = \frac{\gamma}{\Delta\rho g\, R_0}, \tag{2}$$

where $\Delta\rho \equiv \rho_l - \rho_v$ is the difference in mass density between the wetting liquid l and the ambient fluid phase v, while g is the acceleration of gravity.

A. Liquid transport

Two different models for the local transport of wetting liquid between neighboring capillary bridges can be considered. In case the wetting liquid forms a thin film on the surface of the grains, any pair of bridges on the same bead are hydraulic connected. Assuming a quasisteady flow in these films, the total flux between two capillary bridges on the same grain is proportional to the difference in their capillary pressure. The corresponding liquid mobility or conductance coefficient depends on the geometry and distance of the three phase contact lines of the bridges. In addition to the advective transport mechanism, we have to account for a capillary pressure equilibration by mass diffusion of the wetting liquid through the ambient continuous phase. The latter transport mechanism may be effective for wetting liquids with a high vapor pressure or liquids that are partially miscible with the continuous phase.

1. Viscous film flow

For systems in which the nonvolatile liquid forms a wetting film on the surface of the beads, we will regard the average thickness h_0 of the film to be insensitive to the pressure difference P between the wetting liquid and the vapor phase. This assumption is justified whenever the typical horizontal length scales of the roughness are much smaller than the radius of curvature of the menisci in the macroscopic capillary bridges. In addition, we need to assume a sufficiently small microscopic contact angle of the liquid-fluid interface on the rough grain surfaces that permits the formation of a percolating liquid film [1,17].

Assuming a stationary viscous flow in the thin film at any instance in time, the volume flux Q_{ij} between a pair of bridges i and j on the same beads will be proportional to the difference of capillary pressures $P_i - P_j$ and the liquid mobility $\sim h_0^3/\eta$ in the thin film [18]:

$$Q_{ij} = C_{ij}\frac{h_0^3}{\eta}(P_i - P_j), \tag{3}$$

where η is the dynamic viscosity of the wetting liquid, h_0 is the thickness of the wetting film, and $P_{i,j}$ is the Laplace pressure of the two neighboring bridges. Here, we assume that pressure gradients occur over a typical distance of the order $\sim R_0$. Similarly, we estimate the circumference of the three-phase contact line of the bridges on a bead to be of the order $\sim R_0$. The dependence on the particular geometry of the neighboring capillary bridges is adsorbed in the dimensionless conductance coefficient C_{ij}, being of the order of unity.

An exact computation of the conductance coefficients requires solutions to the Laplace equation of the local capillary pressure in the film. Dirichlet boundary data for the capillary pressure are given on the contact lines. Conformal mapping

of the surface of the sphere to a plane allows us to reduce the problem to the computation of the capacitance per length of two parallel and infinite cylindrical conductors [19]. This results shows that the dependence on the size and distance of the bridges is at most logarithmic.

2. *Diffusion through ambient fluid*

A rough estimate of the diffusive flux of a volatile wetting liquid through its ambient vapor phase can be derived from Fick's first law [15,16]. In full analogy to the second regime of capillary equilibration in the thin-film model described above, we will assume that the concentration profile of liquid molecules in the vapor phase has already leveled in every single pore of the bead pack. Gradients in the concentration are noticeable only on length scales much larger than the typical dimension of a pore. As shown in the Appendix, we can write Kelvin's equation in the form

$$n_v - n_v^* = \frac{P n_v^{*2}}{p^* n_l^*}, \tag{4}$$

which allows us to express the particle density of liquid molecules n_v in the vapor phase through the vapor pressure p^* and the densities n_v^* and n_l^* at bulk coexistence, and the pressure difference $P \equiv p_l - p_v$ across the curved interface. As shown in the Appendix, Kelvin's equation (4) still holds if we replace the vapor pressure p^* and densities n_v^*, n_l^* at bulk coexistence of the pure phases by the partial vapor pressure $\tilde{p}_v$, and the particle densities $\tilde{n}_v, \tilde{n}_l$ for a given atmospheric pressure p_0 of the gas phase, respectively.

Using Fick's first law, we can express the volume flux of liquid caused by diffusion of liquid molecules between bridge i and j as

$$Q_{ij} = \tilde{C}_{ij} \frac{D n_v^{*2} R_0}{p^* n_l^{*2}} (P_i - P_j), \tag{5}$$

where D is the diffusion constant of molecules in the vapor phase, cf. Sec. IV. The dimensionless prefactor $\tilde{C}_{ij}$ accounts for the specific geometry of the pore space and the bridge interfaces.

In full analogy to the dimensionless conductance coefficient C_{ij} in the viscous film model, we expect the prefactor $\tilde{C}_{ij}$ to be of order unity. A computation of the matrix elements $\tilde{C}_{ij}$ involves solutions of the three-dimensional Laplace equations for the stationary density profiles with Dirichlet boundary data on the liquid-vapor interface of the capillary bridges.

3. *Transport time scales*

In view of the numerical simulations, it is useful to nondimensionalize all relevant physical quantities. In the following, we employ the average bead radius R_0 as a unit of length. Using a pressure rescaling by γ / R_0, the relation (3) for the volume yields a capillary-viscous time scale of the form

$$T_\mathrm{v} \equiv \frac{\eta R_0^4}{\gamma h_0^3} \tag{6}$$

for the pressure equilibration by fluid transport through a thin viscous film. Employing the relation (5) instead of (3) leads to a time scale

$$T_\mathrm{d} \equiv \frac{p^* n_l^{*2} R_0^3}{\gamma\, n_v^{*2} D} \tag{7}$$

for a diffusive transport through the vapor phase.

Volume fluxes of both transport modes can be superimposed as long as the linear relations between the respective volume flux and pressure difference, Eqs. (3) and (5), are applicable. This implies that the time scale

$$T_0 = \frac{T_\mathrm{v} T_\mathrm{d}}{T_\mathrm{v} + T_\mathrm{d}} \tag{8}$$

accounts both for flows through thin liquid films and for diffusion through the vapor phase. The corresponding dimensionless characteristic number

$$J \equiv \frac{T_\mathrm{v}}{T_\mathrm{d}} = \frac{D\, \eta\, n_v^{*2} R_0}{p^*\, n_l^{*2} h_0^3} \tag{9}$$

allows us to discriminate between two different transport regimes: for $J \gg 1$, the diffusive transport through the vapor phase dominates, while for $J \ll 1$, the main transport is by viscous flows through the thin wetting film. It has been shown experimentally that both cases may indeed be encountered [20–22]. The central message here is that although the relative importance of the two mechanisms may vary and can be expressed by the value of J, the form of the transport equations remains unchanged. Hence it is sufficient to treat the film flow case, as we will do in what follows.

B. Capillary bridges

As in a previous paper [14], the capillary pressure P of a bridge with volume V spanning a gap with separation S between two beads of equal radius R_0 is interpolated from tabulated values. To account for contact-angle hysteresis, we consider capillary bridges with either pinned or freely moving contact lines. A suitable parameter to describe the position of the pinned contact line of a capillary bridge is the opening angle β; cf. also the sketch in Fig. 1.

The capillary pressure of a bridge is a function $\tilde{P}_0(V,S,\beta)$ for the bridges with pinned contact lines depending on the opening angle β in addition to the volume V and gap separation S. For bridges with a freely sliding contact line and a prescribed contact angle θ, the capillary pressure is expressed as a function $P_0(V,S,\theta)$. In addition to the capillary pressure, we compute the contact angle $\theta(V,S,\beta)$ of bridges with a pinned contact line and the opening angle $\beta(V,S,\theta)$ for those with a sliding contact line. To numerically compute the functions $\tilde{P}_0(V,S,\beta)$, $P_0(V,S,\theta)$, $\theta(V,S,\beta)$, and $\beta(V,S,\theta)$, we employed numerical energy minimizations using the public domain software SURFACE EVOLVER [23], where we considered only axially symmetric interfacial profiles using an effectively two-dimensional representation of the bridge state. The rupture distance of a bridge with fixed volume V is computed from the approximate expression

$$S_0^* = \left(1 + \frac{\theta}{2}\right) V^{1/3} \tag{10}$$

as given by Willet *et al.* [24]. As shown in one of the following works, Ref. [25], Eq. (10) is still a good approximation for

bridges with a pinned contact line provided that the opening angle β is not too small. In this case, the actual contact angle $\theta = \theta(V,S,\beta)$ of the bridge is used in Eq. (10).

To account for the dependence of capillary pressure P on the volume V, the surface-to-surface separation S, and on the individual radii R_i of the two beads $i = 1,2$, we use scaled quantities

$$P(V,S,\theta) = \xi^{-1}\, P_0(\xi^{-3}V,\xi^{-1}\,S,\theta), \tag{11}$$

$$\tilde{P}(V,S,\beta) = \xi^{-1}\, \tilde{P}_0(\xi^{-3}V,\xi^{-1}\,S,\beta), \tag{12}$$

$$S^*(V,\theta) = \xi\, S_0^*(\xi^{-3}\,V,\theta), \tag{13}$$

where the dimensionless factor $\xi \equiv R_c/R_0$ accounts for the Derjaguin mean

$$R_c \equiv \frac{2R_1R_2}{R_1+R_2} \tag{14}$$

of bead radii [24].

C. Contact-angle hysteresis

Roughness or variations in the chemical composition of the surface lead to a history-dependent contact angle [18]. Assuming ideal surfaces with uniform surface heterogeneities, the contact angle θ of a fluid interface in a mechanical equilibrium falls into an interval $[\theta_r,\theta_a]$ limited by the receding and advancing contact angle θ_r and θ_a, respectively. The contact line starts to recede once the local contact angle θ equals θ_r. Likewise, the contact line starts to advance if θ equals θ_a For all intermediate values of $\theta \in [\theta_r,\theta_a]$, the contact line is immobilized, i.e., "pinned." The magnitude of contact-angle hysteresis is defined as the width $\Delta\theta \equiv \theta_a - \theta_r$ of the range of static contact angles.

The sketch in Fig. 1 illustrates the impact of contact-angle hysteresis on the equilibration dynamics for the example of two capillary bridges $i = 1,2$. Starting from an initial state with volumes $V_1^0 > V_2^0$, opening angles $\beta_1^0 > \beta_2^0$, and contact angles $\theta_1^0 = \theta_a$, $\theta_2^0 = \theta_r$ at $t = 0$, the capillary pressure difference $P_1^0 - P_2^0 > 0$ drives a fluid flux $Q_{12} > 0$ through the thin film between bridge 1 and 2. As the total volume of bridge 1 and 2 must be conserved, we have $\dot{V}_1 = -\dot{V}_2 = -Q_{12}$, using the dot as a short-hand notation for the total time derivative. Although bridge 1 is shrinking and bridge 2 is growing, all contact lines remain first in a pinned state ($\beta_1 = \beta_1^0$, $\beta_2 = \beta_2^0$, and $\theta_{1,2} \in [\theta_r,\theta_a]$). Only while approaching the final state at $t \to \infty$ with asymptotically equal pressures $P_1^\infty = P_2^\infty$ do the contact lines become depinned ($\theta_1^\infty = \theta_r$, $\theta_1^\infty = \theta_a$), but still with bridge volumes $V_1^\infty > V_2^\infty$. In the absence of contact hysteresis, one would observe equal final volumes $V_1^\infty = V_2^\infty$.

D. Network model

The dynamics of fluid transport in the static bed of beads is studied in a coarse-grained network model where each capillary bridge forms a node i of the network. The nodes are connected by bonds (i,j), representing the thin film between bridges j and i on the same bead. Mass conservation of the wetting fluid demands that the rate of volume change of bridge i is the sum

$$\dot{V}_i = -\sum_{j\in\mathcal{N}(i)} Q_{ij} = \sum_{j\in\mathcal{N}(i)} C_{ij}\,(P_j - P_i) \tag{15}$$

over the set $\mathcal{N}(i)$ of all bridges j that are connected to bridge i. The relative geometry of a pair of neighboring bridges (i,j), the effect of other bridges, or individual bead radii are collected in the dimensionless conductance coefficient C_{ij}, which is of the order of 1. The logarithmic dependence of C_{ij} on the minimum distance of contact lines applies only to capillary bridges close to coalescence. Since we exclude this exceptional case, we set $C_{ij} = 1$ throughout.

For given derivatives $\dot{V}_i$ of bridge volumes Eq. (15) and gap separations $\dot{S}_i$, we are able to compute the total time derivatives of the opening angle β_i and contact angle θ_i of bridge i. Using the differentials

$$a \equiv \partial_V\beta(V_i,S_i,\theta_i)\,\dot{V}_i + \partial_S\beta(V_i,S_i,\theta_i)\,\dot{S}_i,$$

$$b \equiv \partial_V\theta(V_i,S_i,\beta_i)\,\dot{V}_i + \partial_S\theta(V_i,S_i,\beta_i)\,\dot{S}_i,$$

we can express the time derivatives $\dot{\theta}_i$ and $\dot{\beta}_i$ as

$$\dot{\beta}_i = a, \quad \dot{\theta}_i = 0 \quad \text{for} \quad \begin{cases} a \geqslant 0 & \text{and} \quad \theta_i = \theta_a, \\ a \leqslant 0 & \text{and} \quad \theta_i = \theta_r, \end{cases} \tag{16}$$

$$\dot{\beta}_i = 0, \quad \dot{\theta}_i = b \quad \text{for} \quad \theta_r < \theta_i < \theta_a. \tag{17}$$

The dependence on the gap separation S in the differentials becomes important if the beads are allowed to move relative to each other. In a static packing, however, the angles β_i and θ_i depend on V only.

According to Eqs. (16), the contact line of a bridge i can only slide outward ($\dot{\beta}_i > 0$) for a contact angle $\theta_i = \theta_a$. Capillary bridges with inward sliding contact lines ($\dot{\beta}_i < 0$), however, have to satisfy $\theta_i = \theta_r$. Equations (16) guarantee that the contact angle θ_i cannot become larger than θ_a or smaller than θ_r. The complementary case of an immobilized contact line is taken into account by Eqs. (17): Any intermediate value $\theta_r < \theta_i < \theta_a$ of the contact angle θ_i implies a pinned contact line ($\dot{\beta}_i = 0$).

As a consequence of the dynamics described by Eqs. (16) and (17), the state of a capillary bridge is not uniquely determined by the volume V and separation S. Depending on whether the contact line is advancing, pinned, or receding, we have to employ different expressions for the capillary pressure:

$$P_i = \begin{cases} P(V_i,S_i,\theta_a) & \text{for} \quad \dot{\beta}_i > 0, \\ \tilde{P}(V_i,S_i,\beta_i) & \text{for} \quad \dot{\beta} = 0, \\ P(V_i,S_i,\theta_r) & \text{for} \quad \dot{\beta}_i < 0. \end{cases} \tag{18}$$

The evolution of liquid volume $V_i(t)$, opening angle $\beta_i(t)$, and contact angle $\theta_i(t)$ for each individual bridge i is obtained from an integration of Eqs. (15)–(18).

The dependence of the capillary pressure P on the history of bridge volume V for a fixed separation S is illustrated in Fig. 2. The two flat branches in the sketch in Fig. 2 correspond to the case of an advancing (solid line top) and receding contact line (solid line bottom), while the steep branches (dashed lines) describe the pressure of a capillary bridge with pinned contact lines. Due to the history-dependent dynamics specified in Eq. (16), a capillary bridge moving on the branch corresponding to an advancing contact line can

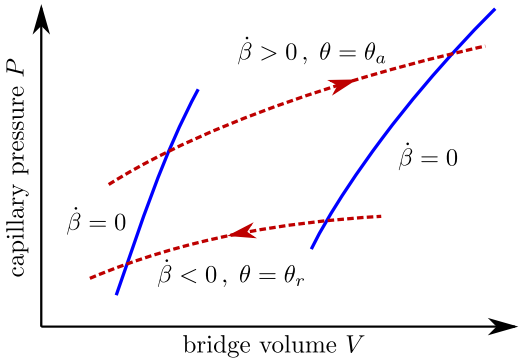

FIG. 2. (Color online) Schematic of the capillary pressure P against the volume V of a bridge. The lower and upper branches (dashed lines) correspond to a receding (lower) and advancing (upper) contact line. The left and right branches (solid lines) describe bridges with a pinned contact line with a small (left) and large (right) opening angle.

be encountered only for growing volumes. Similarly, bridges on the lower branch corresponding to a receding contact line are encountered only for shrinking volumes. In contrast, the volume of a bridge with a pinned contact line can be either growing or shrinking.

A substantial simplification to the full network model Eq. (15) can be obtained by replacing the capillary pressure P_j in Eq. (15) with $j \in \mathcal{N}(i)$ by the mean $\langle P\rangle$ taken over all bridges in the network. The temporal evolution of individual bridge volumes V_i in this "mean-field" approximation is

$$\dot V_i = C\,\langle N_c\rangle(\langle P\rangle - P_i), \tag{19}$$

where C is a global conductance coefficient and $\langle N_c\rangle$ is the average bridge coordination on a bead.

E. Simulations

To reproduce the experimental conditions of the equilibration experiments in Refs. [4,10], we simulate the particle motion during the preparation step using the contact dynamics (CD) algorithm. Since the beads employed in the experiments are a sieving fraction of a wide size distribution, it is reasonable to assume bead radii that are uniformly distributed between a minimum radius, R_-, and a maximum radius, R_+. The degree of polydispersity is parametrized by the ratio $r_{\rm pol} \equiv R_-/R_+ < 1$, while R_+ is employed as our unit of length, R_0. The open simulation box is bounded by a rigid movable wall at the bottom $z = 0$, applying periodic boundary conditions along the x and y directions. Gravity acts on the particles in the $-z$ direction with an acceleration of gravity $g = 9.81\ \mathrm{m/s^2}$.

To create a static packing similar to those in the time-resolved x-ray tomography experiments in Refs. [4,10], the bed of beads is fluidized by an oscillatory motion of the lower wall of the container. The wetting fluid is redistributed exclusively via rupture and formation of capillary bridges. If two beads touch each other, a small bridge is created with $\theta = \theta_a$, where the required minimum fluid volume is provided by all neighboring bridges. Similarly, if the bead separation exceeds the critical distance $S^*(V)$, the bridge ruptures and the volume V is equally split and distributed onto all bridges on the two beads. Capillary forces are small compared to the typical bead mass and acceleration amplitudes during fluidization and are therefore neglected.

Once the agitation is stopped, we let the beads settle by gravity into a mechanically stable packing (setup A). The distribution of fluid volumes obtained with this procedure is close to a decreasing exponential function. To extend our calculations to larger systems while saving the computational costs for the initial preparation, we considered a three-dimensional cubic lattice of beads in contact applying periodic boundary conditions to the box with linear dimensions $L = 200$ (setup B). To mimic the initial state of bridges after the preparation step in A, we initialized the bridges with an exponentially decaying probability distribution function (PDF) of volumes $\propto \exp(-V/\langle V\rangle)$ with a given average volume $\langle V\rangle$, and we set all contact angles $\theta = \theta_a$. To follow the evolution of individual bridge states, we integrated Eqs. (15)–(18) for setups A and B numerically in time using a simple forward Euler time scheme.

III. RESULTS AND DISCUSSION

The simulated evolution of bridge volumes in a static bed of beads after shaking (setup A) is shown in Fig. 3. Following the analysis of the x-ray tomography data in Ref. [10], we classify each bridge according to their binned volume at time $t = 0$. Volume averages over all bridges being in the same bin at $t = 0$ are plotted against the time t elapsed after the agitation has been stopped. To match the parameter of the experiments reported in Ref. [10], we set the polydispersity to $r_{\rm pol} = 0.8$ and chose a total fluid volume corresponding to an overall volume content of $W = 2 \times 10^{-2}$ of the wetting liquid with respect to the total sample volume. The receding contact angle in our simulations is set to $\theta_r = 7^\circ$ throughout, being the smallest value that allows for a reliable interpolation between the tabled functions $P(S,\beta,\theta)$ and $V(S,\beta,\theta)$. The distribution of final bridge volumes for an advancing contact angle $\theta_a = 32^\circ$

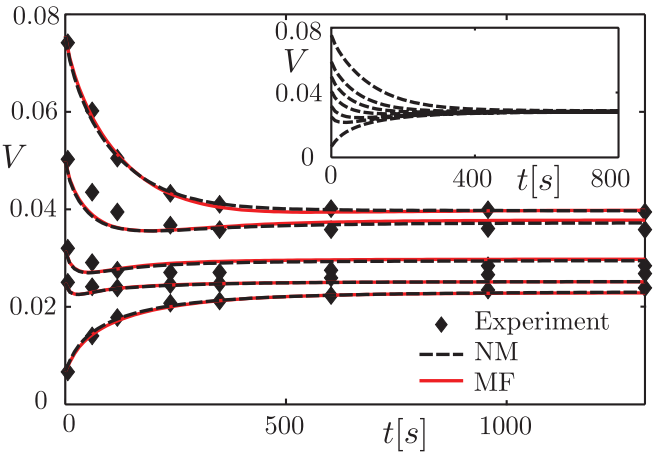

FIG. 3. (Color online) Relaxation of individual capillary bridge volumes as a function of time in experiments (symbols) taken from Ref. [10] and in our simulations for $\Delta\theta = 25^\circ$ in the full network model ("NW," black dashed lines) and the mean-field model ("MF," red solid lines). The inset shows the equilibration dynamics in the network model with $\Delta\theta = 0^\circ$. The receding contact angle is $\theta_r = 7^\circ$ in both cases.

(corresponding to a contact-angle hysteresis of $\Delta\theta = 25^\circ$) provides the best match to the experimental data in Ref. [10].

The plot in Fig. 3 demonstrate that the average bridge volume of a bin does not need to be a monotonously increasing or decreasing function of time. In particular, we observe that some capillary bridges with intermediate volume first shrink for a short time and then tend to grow again. The inset of Fig. 3 shows the case of a vanishing contact-angle hysteresis $\Delta\theta = 0^\circ$, i.e., for contact angles $\theta_a = \theta_r = 7^\circ$. For asymptotically large times, all bridge volumes V_i virtually converge to the same value $\langle V\rangle = V^\infty$. This indicates that the local geometry around contact points and small gaps, i.e., the possible locations of capillary bridges, are very similar. Because the capillary pressure will finally be identical in all bridges, the asymptotic bridge volume V^∞ is determined only by the contact angle, the number of contacts, and the total liquid volume in the granular bed.

A. Transport time scales

In addition to the contact angles θ_a and θ_r, we can employ the time scale T_0 as a free parameter to fit the results of our numerical simulations to the experimental data. The best fit between the data of the equilibration experiments in Ref. [10] and the simulations in setup A shown in Fig. 3 is obtained for $T_0 = 2.1 \times 10^5$ s. Rather unexpectedly, the volume equilibration in setup A appears to be almost completed already after $t \gtrsim 10^{-3}$ expressed in the dimensionless units of our simulations. Rescaling this time by T_0 leads to ≈ 250 s for the crossover, which is corroborated by visual inspection of Fig. 3.

If we assume that the transport proceeds exclusively through viscous flows in thin films, we can employ Eq. (6) to estimate the equivalent thickness of the thin film. Setting the bead radius to $R_0 = 280\ \mu$m, and the interfacial tension and dynamic viscosity of the aqueous ZnI_2 solution to $\gamma = 72$ mN m^{-1} and $\eta = 10^{-3}$ Pa s, respectively, we obtain an estimate of $h_0 = 74$ nm for the effective thickness of the thin wetting film. This value agrees well with the measured rms roughness of glass beads by Utermann *et al.* [26] and the value of h_0 proposed by Lukyanov *et al.* for their system of the nonvolatile liquid Tris(2-ethylhexyl) phosphate in a pack or quartz grains (Ottawa sand) [3].

An estimate of the equilibration time scale T_0 in the presence of a purely diffusive transport in the vapor phase can be obtained from Eq. (7). Assuming pure water as a wetting liquid and ambient conditions with a temperature of 300 K [15,16], we set the vapor pressure to $p^\star = 3.52 \times 10^3$ Pa, the molar densities to $n_l^\star = 5.56 \times 10^4$ mol m^{-3} and $n_v^\star = 1.41$ mol m^{-3}, and the diffusion constant to $D = 2.57 \times 10^{-5}$ m^2 s^{-1}, and we obtain a time scale of $T_d = 6.5 \times 10^7$ s. The low value of the characteristic number $J = 3.23 \times 10^{-3}$ according to Eq. (9) suggests that transport by thin-film flow is favored over diffusive transport in the vapor phase. A further quantitative discussion requires numerical computation of the matrix elements C_{ij} and $\tilde{C}_{ij}$, and it is left to future work.

An additional argument that supports viscous flows as the dominant transport mode in Ref. [10] is due to the high molarity of the aqueous ZnI_2 solution. Any diffusive exchange of only the volatile solvent between bridges, excluding an exchange of the nonvolatile ionic solute, leads to gradients in the chemical potential of the solvent molecules. A simple estimate using Raoult's law demonstrates that any gradient in the chemical potential caused by differences in molarities is large compared to the gradients due to differences in capillary pressure. Hence, a diffusive exchange of bridge volumes is largely suppressed for high salt concentrations.

B. Final volume distribution

An explanation of the width of the final bridge volumes by hydrostatic pressure can be excluded for the equilibration experiments by Scheel *et al.* [10]. Given the interfacial tension γ and density difference $\Delta\rho$ of the 1 M aqueous ZnI_2 solution to the surrounding air, we compute from Eq. (2) a maximal vertical extension of $L_\perp \approx 1$ cm. Since the analyzed field of view in the x-ray tomography imaging had a height of less than $\ell \approx 5$ mm [10], we conclude that only differences in the Laplace pressure were driving the exchange of wetting fluid between neighboring bridges. Gradients of the final distribution of bridge volumes caused by a mismatch in the hydrostatic pressure in the bulk phases will contribute to the width of the volume distribution only if $\ell \gtrsim L_\perp$ holds.

A remaining finite width of the final volume distribution can be related to the degree of polydispersity $r_{\rm pol}$ of bead radii. Figure 4 shows the probability density functions of bridge volumes V obtained in our simulations for a number of size polydispersities $r_{\rm pol}$ at late times. Apparently, all PDFs approach a characteristic triangular shape while their width is increasing as $r_{\rm pol}$ becomes smaller. As expected, the variance of bridge volumes, $\sigma_v \equiv (\langle V^2\rangle - \langle V\rangle^2)^{1/2}$, that quantify the width of the PDFs increases monotonously with $r_{\rm pol}$, the degree of polydispersity (cf. the inset of Fig. 3). This weak sensitivity is a clear indication that the final distributions of volumes observed in the experiments cannot be explained by the polydispersity of bead radii alone. Capillary bridges between spheres not in mechanical contact are rare in packings prepared by setup A, and the PDF of gap separations S between neighboring beads has a negligible impact on the final volume distribution.

An obvious source for the finite width of the final distribution of bridge volumes is a history-dependent contact angle.

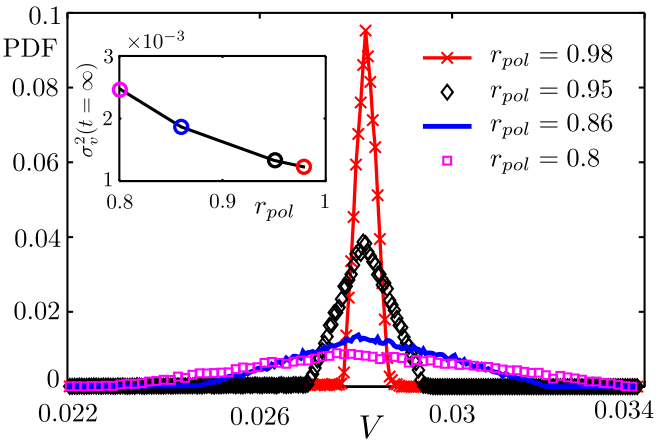

FIG. 4. (Color online) Probability distribution function (PDF) of final bridge volumes V for vanishing contact-angle hysteresis according to setup A. Contact angle $\theta = 7^\circ$. Inset: variance of volumes in the final state for different polydispersities $r_{\rm pol}$.

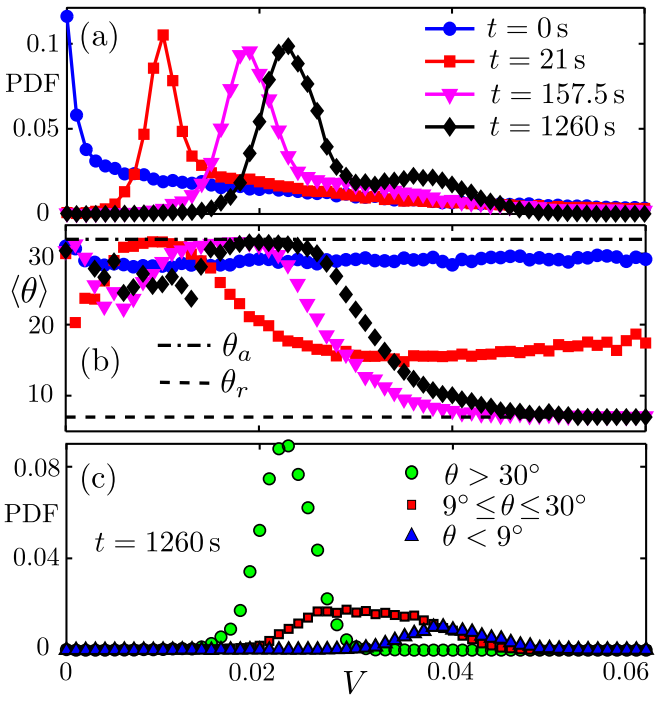

FIG. 5. (Color online) Distributions for data in the network model (NW) shown in Fig. 3: (a) PDF of bridge volume V and (b) average contact angle $\langle\theta\rangle$ of bridges with volume V. (c) PDF to find bridges in bins of contact angles θ close to the advancing, receding, or intermediate range at different times t.

Figure 5(a) shows the PDF of bridge volumes at different times after the agitation has been stopped for a finite contact-angle hysteresis of $\Delta\theta = 25°$. The raising of a second peak in the PDF at large values from an initially monotonously decaying function can be explained by a growing population of bridges with receding contact lines. Shortly after preparation, all bridges exhibit a contact angle close to θ_a, and the average contact angle $\langle\theta\rangle$ of bridges with large volume gradually decreases with time; cf. Fig. 5(b). Bridges with large volume and a capillary pressure close to zero shrink at a smaller rate compared to the rate at which small bridges with advancing contact angles and large negative pressure grow. In the final state, the majority of bridges are still in the advancing state, and they make up for the large peak toward smaller volumes, as can be seen from Fig. 5(c). Most of the remaining bridges exhibit pinned or receding contact lines, accounting for the second, smaller peak toward larger volumes.

C. Large-time asymptotics

Inspection of the direct comparison of the full network model, the mean-field model, and the experimental data of Ref. [10] in Fig. 3 demonstrates that the mean-field model predicts the dynamics for the chosen contact-angle hysteresis of $\Delta\theta = 25°$ at early times rather well. To further assess the range of validity of the mean-field model, and for a quantities comparison of the evolution of capillary pressures and bridge volume at late times, we will now consider the larger setup B.

Figures 6(a) and 6(b) display a comparison of the squares of variances σ_p and σ_v corresponding to the PDF of capillary

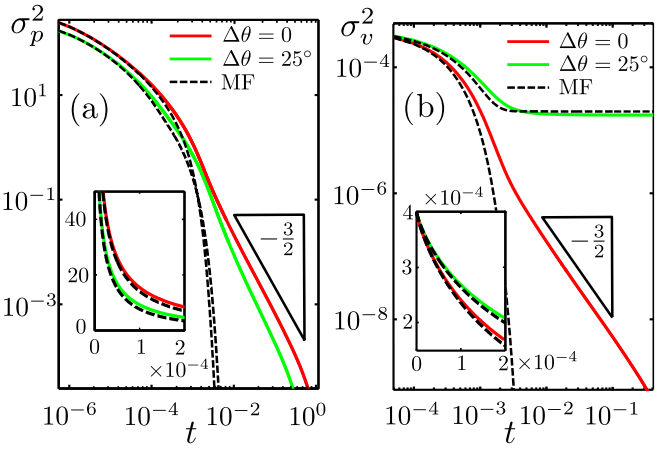

FIG. 6. (Color online) (a) Squared variance of capillary pressure, σ_p^2, and (b) of bridge volumes, σ_v^2, as a function of time t for $\Delta\theta = 0°$ (red solid lines) and $\Delta\theta = 25°$ in the network model and in the mean-field approximation (dashed lines) for setup B. Insets show the same data at early times in linear scale.

pressure P and bridge volume V, respectively, in the mean-field model (dashed lines) and the full network model (solid lines). In contrast to the data shown in Fig. 3, we use the nondimensionalized time in Fig. 6. As for the simulations of setup A, we chose a contact-angle hysteresis of $\Delta\theta = 0°$ (red solid lines) and 25° (green solid lines).

In the case of a vanishing contact-angle hysteresis, we find a power-law decay of both σ_p^2 and σ_v^2 in t with an exponent $-3/2$, as expected for continuum models for linear diffusion in three spatial dimensions [27]; cf. the red solid lines in Figs. 6(a) and 6(b). The crossover from the initial exponential decay to the power-law decay can be observed at an estimated time $t = \tau_e \approx 10^{-3}$. This is in good agreement with the dimensionless crossover time observed in experiments and in setup A. At early times $t \ll \tau_e$, the observed evolution of both σ_p^2 and σ_v^2 in the full network model is well captured by the mean-field model. This is not surprising as the capillary pressure of bridges is not correlated immediately after the initialization. The buildup of spatial correlations in the capillary pressure at later times $t \gg \tau_e$ will invalidate the mean-field model.

The decay of the squared variance σ_p^2 for a contact-angle hysteresis $\Delta\theta = 25°$ is slightly faster than that for the case of vanishing contact-angle hysteresis [cf. the green and red solid line in Fig. 6(a)]. A pronounced qualitative difference, however, is observed for the squared variance of volumes σ_v^2, displayed as the green and red solid lines in Fig. 6(b).

Inspection of Fig. 6(b) shows that the volume fluctuations in the initial bridge volume do not fully decay in the limit $t \to \infty$ if the contact-angle hysteresis is set to the finite value $\Delta\theta = 25°$. Instead, the variance of bridge volumes shown by the green solid curve in Fig. 6(b) saturates to a value $\sigma_v^2(t = \infty) > 0$. Apparently, the time at the crossover and the level of the plateau are reasonably well captured by the mean-field model (dashed black line). Here, we would expect to observe a breakdown of the mean-field model at late times because the capillary pressure fluctuations become correlated irrespective of the magnitude of contact-angle hysteresis. The history dependence of the contact angle, however, prevents a

buildup of large correlations in the fluctuations of neighboring bridge volumes. The time of the crossover of σ_v^2 to the plateau is comparable to τ_e obtained from simulations for $\Delta\theta = 0°$.

D. Crossover time

The crossover time τ_e for the case without contact-angle hysteresis can be related to the time when the capillary pressure of neighboring bridges starts to be correlated. To obtain an estimate for τ_e, we employ the continuum picture of a mode expansion of volume fluctuations into a spectrum of modes with short and long wavelengths. Similar arguments have been applied to determine the crossover time of diffusive solvent transport in a network of densely packed emulsion droplets [27]. Provided the equilibration dynamics is described by a linear equation, we can think of the spatial fluctuations of bridge volumes as a superposition of modes in the local liquid saturation c. According to the Nyquist-Shannon sampling theorem [28], the shortest meaningful wavelength of such a mode $c(\mathbf{r},t)$ is given by twice the smallest distance of two neighboring bridges. Toward large wavelengths, the spectrum is limited by the system size L.

Solutions of the linear diffusion equation, $D_e \Delta c = \partial_t c$, with the three-dimensional Laplacian Δ and the effective diffusion constant D_e, show that amplitudes $c_{\mathbf{q}}$ of a mode $c(\mathbf{r},t) = c_{\mathbf{q}} \exp(i\mathbf{q}\cdot\mathbf{r} - t/\tau_{\mathbf{q}})$ decay exponentially with a time scale $\tau_{\mathbf{q}} = D_e^{-1}\,|\mathbf{q}|^{-2}$. The characteristic decay time of the mode with the largest wave number $q_{\max}$ provides us with an estimate of τ_e. Employing $2R_0$ as the typical distance between two neighboring bridges, we have $q_{\max} \approx \pi/4R_0$.

An estimate of the effective diffusion constant D_e can be obtained from the link between the continuum diffusion equation and the discrete network model Eq. (15). Considering the right-hand side of Eq. (15) as an approximation of the Laplace operator, we need to correct the left-hand side of (15) for a numerical prefactor given by the coordination of neighboring bridges for a proper mapping onto the continuum diffusion equation. For the regular bridge network of setup B, we find a number of $N_c = 10$ neighbors. When expanding the capillary pressure P_i in the volume fluctuation around the final volume V^∞ up to linear order, we obtain a linear diffusion equation for the fluctuations of the saturation field $c(\mathbf{r},t)$.

After collecting all factors, we find that the effective diffusion constant D_e of volume fluctuation in the bridge network is given by an expression

$$D_e \approx C\,\frac{N_c}{2d}\,\frac{\partial P}{\partial V}\bigg|_{V=V^\infty}, \tag{20}$$

where d is the spatial dimension of the bridge network. Setting global parameters separation $S = 0$, contact angle $\theta = 7°$, asymptotic volume $V^\infty \approx 0.02$, and the conductance coefficient $C = 1$, we obtain an estimated effective diffusion constant $D_e \approx 500$ and a corresponding time scale $\tau_e \approx 10^{-3}$ that compares well with the observed crossover time in the simulation of setup B; cf. the beginning of Sec. III A. We find a faster diffusive spreading in the network with a diffusion constant $D_e \approx 10^3$ if we consider capillary bridges with a pinned contact line and opening angle $\beta = 21.5°$ (corresponding to a volume of $V^\infty = 0.02$). We obtain this estimate by replacing the capillary pressure P in Eq. (20) for bridges with freely sliding contact lines at a fixed contact angle with the pressure $\tilde{P}$ for bridges with pinned contact lines. An enlarged value of the derivatives of the capillary pressure with respect to the volume is also apparent in the sketch in Fig. 2. The accelerated diffusive transport of liquid in the capillary bridge network with pinned contact lines becomes even more pronounced for larger contact angles.

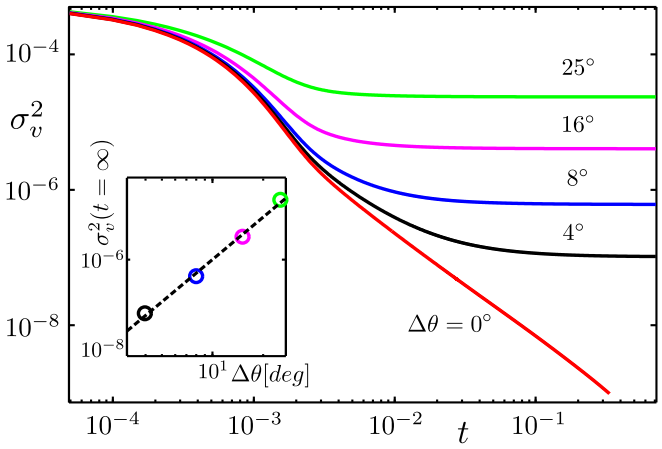

FIG. 7. (Color online) Temporal evolution of the squared variance σ_v^2 of bridge volumes in the full network model for different magnitudes of contact-angle hysteresis, $\Delta\theta = 0°, 4°, 8°, 15°, 25°$. Inset: double logarithmic plot of $\sigma_v^2(t=\infty)$ against $\Delta\theta$ in comparison to a power law $\sim\Delta\theta^3$ (dashed line).

So far, we have explored the differences in the late-time regimes of equilibration of bridge volume for the two extreme cases of a large contact-angle hysteresis $\Delta\theta = 25°$ and vanishing hysteresis. A crossover to a power-law scaling of the variance of bridge volumes observed for the ideal case $\Delta\theta = 0°$ can be understood in the framework of a continuum model for diffusion. To quantify the intermediate cases, we considered the late-time regimes for a series of contact-angle hysteresis. Figure 7 shows the decay of the square of the volume variance, σ_v^2, for additional values $\Delta\theta = 4°, 8°, 15°$ in setup B. The plot in the inset of Fig. 7 displays the value $\sigma_v^2(t=\infty)$ at saturation in a double logarithmic plot. The available data suggest a power law of $\sigma_v^2(t=\infty) \propto \Delta\theta^3$ that needs to be confirmed in further investigations, including larger regions of the parameter space.

IV. OUTLOOK AND CONCLUSIONS

The present numerical study demonstrates that contact-angle hysteresis strongly affects the evolution and distribution of capillary bridge volumes after mixing a wetting fluid into a bed of spherical beads. Our model study shows that disorder of the local geometry in the granular bed, such as the distribution of gap separations and the polydispersity of bead radii, hardly contributes to the final width of bridge volume distribution. Unless the difference between the advancing and receding contact angle on the beads is unrealistically small, contact-angle hysteresis will always dominate the final distribution of bridge volumes.

Our numerical results further demonstrate that a mean-field model for the capillary pressure is sufficient to describe the equilibration process at early times. A reliable prediction

of the final distribution of bridge volumes, however, must account for the network of communicating bridges. The time of the crossover between the early-time regime with negligible spatial correlations of the volume fluctuations to a late-time regime where a continuum model describes the volume distribution can be derived for the ideal case of a vanishing contact-angle hysteresis. This crossover time provides an estimate for the saturation time of spatial volume fluctuations in the case of high contact-angle hysteresis.

The network model can be further employed to address the role of contact-angle hysteresis in fluid transport in slowly sheared granular beds, or the dynamics of liquid equilibration in particulate materials driven by gradients in the local saturation. It can be easily extended to account for flows of the wetting fluid induced by gravity or evaporation.

ACKNOWLEDGMENTS

We thank Mario Scheel and Jean-Christophe Baret for fruitful discussions, and we acknowledge funding by the German Research Foundation (DFG) through the Grants No. He 2732/11-3 and No. He 2016/14-3 in the SPP 1486 "PiKo". This work was also supported by Grant No. FP7-319968 Flow-CCS of the European Research Council (ERC) advanced grant.

APPENDIX

The starting point for the derivation of Eqs. (4) and (5) for a one-component system is the condition of coexistence

$$\mu_v(p_v,T) = \mu_l(p_l,T) \tag{A1}$$

for the chemical potential μ_i of bulk phases $i \in \{v,l\}$ at temperature T. Due to the curved interface between the liquid and vapor phase, we have $p_l \neq p_v$. Expanding the chemical potential $\mu_i(p,T)$ of the liquid and vapor phase around the pressure $p^\star$ at coexistence with a flat interface leads to

$$\Delta\mu_i(p_i,T) \approx \mu^*(T) + \left.\frac{\partial\mu_i}{\partial p}\right|_{p=p^*} \Delta p_i, \tag{A2}$$

with $\Delta p_i = p_i - p^*$.

Maxwell's relation for the grand potential $G_i(p_i,N,T) = N_i\mu_i(p_i,T)$ of the bulk phases $i \in \{v,l\}$ provides us with the expression

$$\frac{\partial\mu_i}{\partial p} = \frac{1}{n_i} \tag{A3}$$

for the molar density n_i of the bulk phases, and we can rewrite Eq. (A2) in the form

$$p_l - p_v = \frac{n_l^* - n_v^*}{n_v^*}\,\Delta p_v \approx \frac{n_l^*}{n_v^*}\,\Delta p_v, \tag{A4}$$

where the preceding approximation is justified as long as $n_l^*/n_v^* \gg 1$ holds. Since we assume the dilute vapor to be an ideal gas, we can employ the relation $p_v/p^* = n_v/n_v^*$ and rewrite Eq. (A4) in the form

$$n_v - n_v^* = \frac{P\,n_v^{*2}}{p^*\,n_l^*}, \tag{A5}$$

in terms of the capillary pressure $P \equiv p_l - p_v$. Equation (A5) is equivalent to Kelvin's equation.

In most cases, the liquid coexists with a mixture of the liquid vapor and an inert gas that is insoluble in the liquid phase. In this case, we need to replace the equilibrium condition Eq. (A1) by

$$\mu_v(p_v,T) = \mu_l(p_0 + P,T), \tag{A6}$$

where p_0 is the ambient atmospheric pressure, and $\tilde{p}_v$ is the partial pressure of the liquid vapor. An expansion of both sides of Eq. (A6) around the partial vapor pressure $\tilde{p}_v$ of a flat interface defined by

$$\mu_v(\tilde{p}_v,T) = \mu_l(p_0,T) \tag{A7}$$

provides us with the Kelvin equation

$$n_v - \tilde{n}_v = \frac{P\tilde{n}_v^2}{\tilde{p}_v\tilde{n}_l}, \tag{A8}$$

which is of the same form as Eq. (A5). All bulk quantities occurring in Eq. (A8), however, refer to a constant ambient pressure p_0 of the gas phase.

According to Fick's first law of diffusion, the current $\mathbf{j}$ of liquid molecules in the vapor phase can be related to the concentration gradient ∇n_v and the diffusion constant D by

$$\mathbf{j} = -D\nabla n_v. \tag{A9}$$

Since the total particle current $\dot{N}_{ij}$ between bridge i and j scales with the interfacial area of the bridges $\sim R_0^2$ and with the gradient $|\nabla| \sim R_0^{-1}$, we finally arrive at a volume flux of the liquid phase,

$$Q_{ij} = \tilde{C}_{ij}\frac{D\,n_v^{*2}\,R_0}{p^*\,n_l^{*2}}\,(P_i - P_j), \tag{A10}$$

where R_0 is the bead radius and $\tilde{C}_{ij}$ is a numerical prefactor that accounts for the particular geometry of the bridges and pore space.

[1] S. Herminghaus, *Wet Granular Matter: A Truly Complex Fluid*, Series in Soft Condensed Matter Vol. 6 (World Scientific, Singapore, 2013).

[2] N. Fernandez, R. Mani, D. Rinaldi, D. Kadau, M. Mosquet, H. Lombois-Burger, J. Cayer-Barrioz, H. J. Herrmann, N. D. Spencer, and L. Isa, Phys. Rev. Lett. **111**, 108301 (2013).

[3] A. V. Lukyanov, M. M. Sushchikh, M. J. Baines, and T. G. Theofanous, Phys. Rev. Lett. **109**, 214501 (2012).

[4] M. Scheel, R. Seemann, M. Brinkmann, M. Di Michiel, A. Sheppard, B. Breidenbach, and S. Herminghaus, Nat. Mater. **7**, 189 (2008).

[5] S. Herminghaus, Adv. Phys. **54**, 221 (2005).

[6] M. Kohonen, D. Geromichalos, M. Scheel, C. Schier, and S. Herminghaus, Physica A **339**, 7 (2004).
[7] E. Teunou and D. Poncelet, J. Food Eng. **53**, 325 (2002).
[8] S. J. R. Simons and R. J. Fairbrother, Powder Technol. **110**, 44 (2000).
[9] J. Litster and B. Ennis, *The Science and Engineering of Granulation Processes*, Particle Technologies Series (Kluwer Academic, Dordrecht, The Netherlands, 2004).
[10] M. Scheel, R. Seemann, M. Brinkmann, M. Di Michiel, A. Sheppard, and S. Herminghaus, J. Phys.: Condens. Matter **20**, 494236 (2008).
[11] M. Jean and J. J. Moreau, *Contact Mechanics International Symposium* (Presses Polytechniques et Universitaires Romandes, Lausanne, 1992).
[12] J. J. Moreau, Eur. J. Mech. A-Solid **13**, 93 (1994).
[13] L. Brendel, T. Unger, and D. E. Wolf, *The Physics of Granular Media* (Wiley-VCH, Weinheim, 2004), pp. 325–343.
[14] R. Mani, D. Kadau, D. Or, and H. J. Herrmann, Phys. Rev. Lett. **109**, 248001 (2012).
[15] E. Shahraeeni and D. Or, Langmuir **26**, 13924 (2010).
[16] E. Shahraeeni and D. Or, Water Resour. Res. **48**, W05511 (2012).
[17] S. Herminghaus, Phys. Rev. Lett. **109**, 236102 (2012).
[18] P.-G. De Gennes, F. Brochard-Wyart, and D. Quéré, *Capillarity and Wetting Phenomena: Drops, Bubbles, Pearls, Waves* (Springer, New York, NY, 2004).
[19] A. T. Adams, *Electromagnetics for Engineers* (Ronald, New York, 1962).
[20] H. Musil, S. Herminghaus, and P. Leiderer, Surf. Sci. Lett. **294**, 919 (1993).
[21] S. Herminghaus, T. Paatzsch, T. Häcker, and P. Leiderer, Europhys. Lett. **31**, 157 (1995).
[22] R. Seemann, W. Mönch, and S. Herminghaus, Europhys. Lett. **55**, 698 (2001).
[23] K. Brakke, Philos. Trans. R. Soc. London, Ser. A **354**, 2143 (1996).
[24] C. D. Willet, M. J. Adams, S. A. Johnson, and J. P. K. Seville, Langmuir **16**, 9396 (2000).
[25] C. D. Willet, M. J. Adams, S. A. Johnson, and J. P. K. Seville, Powder Technol. **130**, 63 (2003).
[26] S. Utermann, P. Aurin, M. Benderoth, C. Fischer, and M. Schröter, Phys. Rev. E **84**, 031306 (2011).
[27] Y. Skhiri, P. Gruner, B. Semin, Q. Brosseau, D. Pekin, L. Mazutis, V. Goust, F. Kleinschmidt, A. El Harrak, J. B. Hutchison, E. Mayot, J.-F. Bartolo, A. D. Griffiths, V. Taly, and J.-C. Baret, Soft Matter **8**, 10618 (2012).
[28] J. W. Goodman, *Introduction to Fourier Optics* (McGraw-Hill, New York, 1968).